The Astrophysical Journal, 747:77 (12pp), 2012 March 1 doi:10.1088/0004-637X/747/1/77

SYSTEMATIC UNCERTAINTIES IN THE SPECTROSCOPIC MEASUREMENTS OF NEUTRON-STAR MASSES AND RADII FROM THERMONUCLEAR X-RAY BURSTS. II. EDDINGTON LIMIT

Tolga Güver[1], Feryal Özel, and Dimitrios Psaltis
Department of Astronomy, University of Arizona, 933 North Cherry Avenue, Tucson, AZ 85721, USA
Received 2011 April 14; accepted 2011 December 20; published 2012 February 15

ABSTRACT

Time-resolved X-ray spectroscopy of thermonuclear bursts observed from low-mass X-ray binaries offer a unique tool to measure neutron-star masses and radii. In this paper, we continue our systematic analysis of all the X-ray bursts observed with *Rossi X-ray Timing Explorer* from X-ray binaries. We determine the events that show clear evidence for photospheric radius expansion and measure the Eddington limits for these accreting neutron stars using the bolometric fluxes attained at the touchdown moments of each X-ray burst. We employ a Bayesian technique to investigate the degree to which the Eddington limit for each source remains constant between bursts. We find that for sources with a large number of radius expansion bursts, systematic uncertainties are at a 5%–10% level. Moreover, in six sources with only pairs of Eddington-limited bursts, the distribution of fluxes is consistent with a ∼10% fractional dispersion. This indicates that the spectroscopic measurements of neutron-star masses and radii using thermonuclear X-ray bursts can reach the level of accuracy required to distinguish between different neutron-star equations of state, provided that uncertainties related to the overall flux calibration of X-ray detectors are of comparable magnitude.

Key words: stars: neutron – X-rays: binaries – X-rays: bursts

Online-only material: color figures

1. INTRODUCTION

Measurements of the masses and radii of neutron stars provide some of the most direct constraints on the equation of state of the matter in the cores of these compact objects. Time-resolved X-ray spectroscopy of thermonuclear bursts observed from some of the low-mass X-ray binaries has been one of the observational methods to constrain the neutron-star masses and radii (see, e.g., van Paradijs 1978, 1979; Damen et al. 1990; Lewin et al. 1993). The method involves modeling high time resolution, high signal-to-noise X-ray burst data to spectroscopically measure the apparent radius and the Eddington luminosity for the neutron star, both of which are related to its mass and radius.

The first few seconds of some of the brightest X-ray bursts show a characteristic pattern in which the color temperature increases and then decreases, while the apparent radius monotonically increases (see, e.g., Galloway et al. 2008a). Eventually, the apparent radius starts to decrease as the color temperature reaches a peak and the burst starts to decay. In the meantime, the flux remains nearly constant at a peak value. This phenomenon is understood as the response of the outermost layers of the neutron star to a super-Eddington burst flux, where the photosphere expands to a few times the stellar radius and subsequently contracts back to the neutron-star surface. During the expansion and the contraction phase, the X-ray flux stays very close to the Eddington limit and any excess energy is transferred into kinetic energy of the outflow (see, e.g., Kato 1983; Ebisuzaki et al. 1983; Paczynski & Proszynski 1986). Accordingly, X-ray bursts from which this phenomenon is observed are called photospheric radius expansion (PRE) events, and the fluxes attained during the expansion episodes of these bursts are used as a measure of the local Eddington limit of the neutron star (van Paradijs 1978), where the gravitational and radiation forces are balanced.

PRE events can be used to determine the Eddington luminosity if the distance to the X-ray binary is known (see, e.g., Basinska et al. 1984; Damen et al. 1990; Kuulkers et al. 2003; Galloway et al. 2008a, 2008b). Using the X-ray bursters located in globular clusters and the peak fluxes reached during X-ray bursts, Kuulkers et al. (2003) tested the idea that the PRE events can be used as a standard candle. They found that the peak fluxes attained during the PRE events can indeed be used as standard candles and are accurate to at least within 15%. Similarly, using 66 and 40 X-ray bursts from 4U 1728−34 and 4U 1636−536, respectively, Galloway et al. (2003, 2006) found that the peak fluxes reached during PRE events are normally distributed with a standard deviation of ≈3% and 7.6%, respectively, after corrections related to the orbital modulation and the composition of the atmosphere are applied.

Even though a measurement of the Eddington limit of an accreting neutron star is useful toward measuring its mass and radius, the determination of the exact moment when a given X-ray burst reaches this limit is not always straightforward. The observed X-ray flux during the PRE episode is expected to vary owing to changes in the gravitational redshift as the apparent photospheric radius rises and falls (see, e.g., Damen et al. 1990). The first moment the flux reaches the Eddington limit occurs during the burst rise and is not always robustly identified for all of the bursts. Alternatively, the Eddington limit can be measured at the moment when the photosphere "falls" back to the neutron-star surface. This has been called the touchdown moment (Damen et al. 1990) and is identified as the point at which the blackbody temperature reaches the highest value during the burst while the apparent radius is lowest. Combined with a measurement of the distance and apparent angular size of the neutron star, the measurement of the Eddington flux at touchdown can lead to uncorrelated measurements of the neutron-star mass and radius (see, e.g., Ebisuzaki 1987; Damen et al. 1990; Özel et al. 2009; Güver et al. 2010a, 2010b).

Nearly continuous observations of bursting low-mass X-ray binaries over the last 15 years with the *Rossi X-ray*

[1] Current address: Sabancı University, Faculty of Engineering and Natural Sciences, Orhanlı-Tuzla, Istanbul 34956, Turkey.

Timing Explorer (*RXTE*) provided high-quality data for over 1000 X-ray bursts from more than 40 X-ray binaries (Galloway et al. 2008a). This rich database of X-ray burst observations enables a study of the spectra of PRE bursts from which the Eddington limit can be measured and any systematic variations in the inferred spectral parameters of the X-ray bursts can be inferred. Such an assessment is essential to better establish the reliability of the mass and radius measurements from time-resolved spectroscopic analysis of X-ray bursts.

Using the archival *RXTE* observations, we recently studied the systematic uncertainties present in the apparent radius measurements during the cooling tails of the X-ray bursts (Güver et al. 2012, hereafter Paper I). Our analysis showed that the vast majority of the X-ray spectra extracted from the cooling tails of 447 X-ray bursts are statistically consistent with Planckian functions and the inferred spectral parameters for the majority of the bursts follow the expected $F \propto T^4$ relation for most of the sources. These results enabled us to measure the apparent radii of a number of neutron stars and assess the systematic uncertainties in these measurements.

In this paper, we continue to analyze all of the X-ray bursts observed from low-mass X-ray binaries in order to determine the uncertainties related to spectroscopic measurements of the Eddington limit in PRE bursts. We focus on the measurement of the Eddington flux at the touchdown moments in 12 X-ray binaries from which multiple PRE events have been observed. Our aim is to determine any systematic uncertainties in these measurements.

In Section 2, we briefly summarize the observations and data analysis techniques, which we discuss in full detail in Paper I. In Section 3, we introduce a systematic method to select the PRE events from the burst archive using time-resolved spectroscopic measurements. In Sections 4 and 5, we describe the statistical tools based on Bayesian Gaussian mixture algorithms that we use to determine the Eddington limit and associated systematic uncertainties for each source. Finally, in Section 6, we present our results and discuss their implications.

2. OBSERVATIONS AND DATA ANALYSIS

Galloway et al. (2008a) presented a catalog of *RXTE* observations of X-ray bursts from 48 low-mass X-ray binaries. Following Paper I, we chose 12 X-ray binaries from this sample based on a number of criteria. We included only the sources that show at least two PRE events (as defined in Galloway et al. 2008a). We excluded all X-ray binaries that are known to be dippers, accretion disk corona sources, or have high inclinations, as well as the known millisecond pulsars. Because they are likely to be affected by source confusion (Galloway et al. 2008a; Keek et al. 2010), we excluded observations of GRS 1741.9−2853 and 2E 1742.9−2929 and also a small number of bursts from Aql X-1, 4U 1728−34, and 4U 1746−37. Finally, since studies of the PRE events observed from EXO 1745−248, 4U 1608−52, and 4U 1820−30 have been reported elsewhere (Özel et al. 2009; Güver et al. 2010a, 2010b), the results for these sources will not be repeated here.

As in Paper I, we imposed a limit on the persistent flux measured prior to each X-ray burst such that it does not exceed 10% of the peak burst flux, i.e., $\gamma \equiv F_{\rm per}/F_{\rm Edd} < 0.1$ as calculated by Galloway et al. (2008a). Imposing this limit reduces the systematic uncertainties introduced by subtracting the pre-burst emission from the X-ray burst spectra.

The final list of all the X-ray binaries and the X-ray bursts we studied is presented in Table 1. We performed the data analysis following the methods detailed in Galloway et al. (2008a) and in Paper I. We extracted time-resolved 2.5–25.0 keV X-ray spectra from all the *RXTE*/Proportional Counter Array (PCA) layers. We varied the exposure time between 0.25 s and 1 s to keep the signal-to-noise ratio constant based on the count rate during the burst. We also used a 16 s spectrum, obtained prior to each burst, as background. Response matrix files were generated using the PCARSP version 11.7, HEASOFT release 6.7, and HEASARC's remote calibration database. We took into account the offset pointing of the PCA during the creation of the response matrix files. Finally, we corrected all of the X-ray spectra for PCA dead time following the method suggested by the *RXTE* team.[2]

We used the Interactive Spectral Interpretation System, version 1.4.9-55 (Houck & Denicola 2000), and custom built S-Lang[3] scripts for spectral analysis. We fit each spectrum with a blackbody function using the *bbodyrad* model (as defined in XSPEC; Arnaud 1996) and with *tbabs* (Wilms et al. 2000) to model the interstellar extinction. For each source, we fixed the hydrogen column density ($N_{\rm H}$) to the values given in Table 1 of Paper I. In the same analysis, we also determined that the level of systematic uncertainty required to make the X-ray burst spectra of each source consistent with blackbody functions is less than 5% (see Section 3.1 and Table 2 in Paper I for details). During each fit, we included these minor systematic uncertainties that we inferred for each source. We then created for each burst that has high temporal and spectral data coverage a time series of blackbody temperatures T_c (units of keV) and normalizations A (in units of [km/10 kpc]^2) throughout the burst that resulted from the time-resolved spectral analysis. We used Equation (3) of Galloway et al. (2008a) to calculate the bolometric fluxes. In the following sections, we adopted the burst numbering system introduced by Galloway et al. (2008a).

Table 1
The Number of PRE Events for Each Source

Name	Number of Bursts[a]	Catalog PRE[b]	γ Limit[c]	$n_{\rm PRE}$
4U 0513−40	7	2	2	2
4U 1636−53	172	52	49	46
4U 1702−429	47	6	6	1
4U 1705−44	47	4	4	2
4U 1724−307	3	3	3	2[d]
4U 1728−34	106	80	71	16
KS 1731−260	27	6	4	2
4U 1735−44	11	8	4	2
4U 1746−37	30	3	0	...
SAX J1748.9−2021	16	8	3	2
SAX J1750.8−2900	4	2	2	2
Aql X-1	57	10	10	6

Notes.
[a] Values are adopted from Galloway et al. (2008a) and show the total number of X-ray bursts detected by *RXTE*.
[b] The total number of X-ray bursts tagged as PRE or potentially PRE events in the Galloway et al. (2008a) catalog.
[c] The number of remaining bursts with peak flux that exceeds the pre-burst emission by a factor of 10.
[d] As discussed in detail in Paper I, we excluded the first burst observed from 4U 1724−307 from our analysis, since model fits of the X-ray spectra extracted from this burst cannot be fitted with a Planckian function and addition of absorption edges at several energies is needed (in't Zand & Weinberg 2010).

[2] ftp://legacy.gsfc.nasa.gov/xte/doc/cook_book/pca_deadtime.ps
[3] http://www.jedsoft.org/slang/

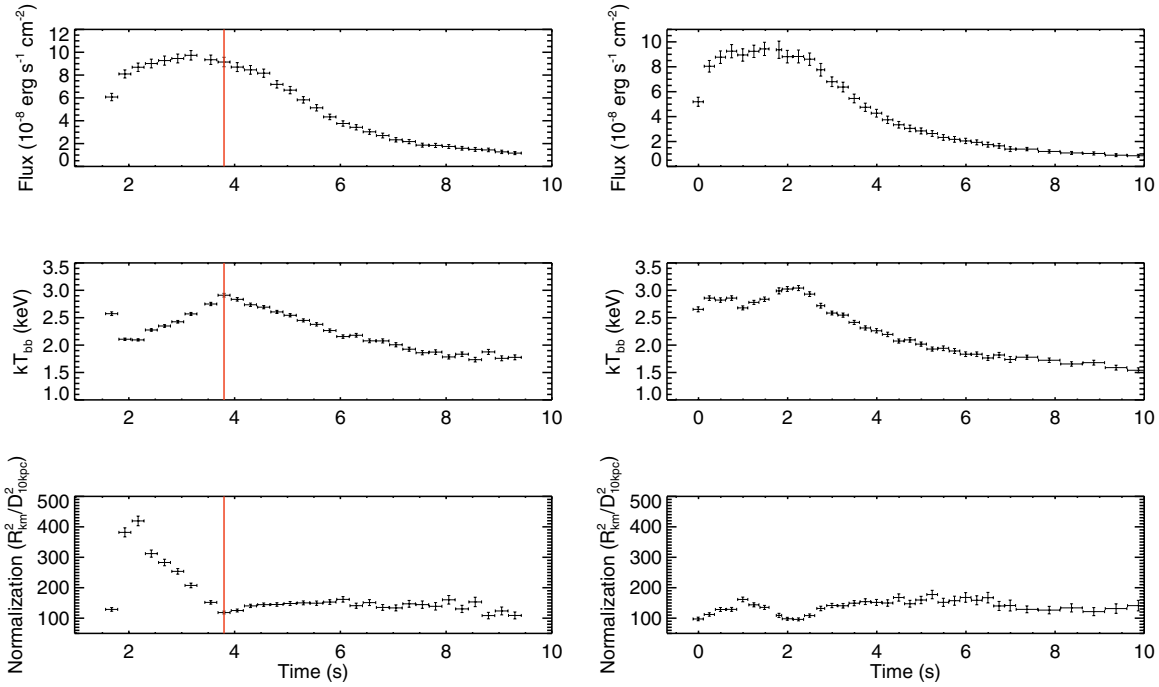

Figure 1. Examples of X-ray bursts observed from 4U 1728−34. The left panel shows burst 86, which satisfies our criteria for PRE identification summarized in Section 3. The right panel shows burst 104, which does not satisfy the criteria and hence is not labeled as a PRE event. The selected touchdown moment for the PRE event is also shown by a vertical line.

(A color version of this figure is available in the online journal.)

3. DETERMINATION OF PHOTOSPHERIC RADIUS EXPANSION EVENTS

Our first aim is to select the PRE bursts in the X-ray burst sample, so that we can use the fluxes attained in them as a measure of the local Eddington limit on the neutron-star surface. As a signature of PRE, we look specifically for a significant increase in the measured blackbody radius in the burst rise and a following decrease, in bursts where the X-ray flux remains almost constant at a peak value. Galloway et al. (2008a) devised a set of criteria based on the spectral parameter variation in each burst in order to identify PRE events and to differentiate them from other typical X-ray bursts. We adopt and augment these criteria, as we discuss below.

Galloway et al. (2008a) took the following measures as evidence that a radius expansion occurred: (1) the blackbody normalization A reached a (local) maximum close to the time of peak flux, (2) lower values of the normalization A were measured following the maximum, with the decrease significant to 4σ or more, and (3) there was evidence of a (local) minimum in the fitted temperature T_c at the same time as the maximum in A. In Figure 1, we show examples of the spectral evolution of two different bursts that satisfy these criteria. While the burst in the left panel is a clear PRE event, with the photosphere at the peak flux reaching many times the neutron-star radius in the cooling tail, the event on the right shows a higher normalization late in the burst than it does during the assumed photosphere expansion. In fact, the blackbody normalization during the early local maximum is smaller than the asymptotic normalization of even non-PRE bursts during their cooling tails. We, therefore, conclude that the latter example is not a secure PRE event.

In order to eliminate such cases, we added an additional criterion that is based on the comparison of the peak blackbody normalization reached during an X-ray burst, $A_{\rm peak}$, with the measurement of the average normalization, $A_{\rm cool}$, found from the cooling tail for each source. For the former quantity, $A_{\rm peak}$, we select the peak normalization that occurs when the measured flux is higher than half of the peak flux. This flux limit ensures that the peak normalization is selected when the PRE is expected to occur. For the latter quantity, $A_{\rm cool}$, we used the average value found from the cooling tails of all the bursts for each source as reported in Paper I. Note that for Aql X-1 and 4U 0513−401, large systematic uncertainties present in the cooling tails prevented a reliable measurement of their apparent radii in Paper I. Because of that, we used approximate values of $R/D = 14.6$ km/10 kpc and $R/D = 5.7$ km/10 kpc, respectively, which correspond to the highest flux bins of their cooling tails.

In Figure 2, we show the histogram of all the normalization ratios $A_{\rm peak}/A_{\rm cool}$ for all the bursts observed from all the sources included in this study. The resulting histogram shows that the distribution of the ratio of the peak normalization to the apparent radius has a main peak around unity and an extended tail toward higher values. The high peak around unity at the peak normalization shows that, for the majority of the X-ray bursts, the burning covers the apparent surface area of the neutron star found from the cooling tails. However, there are a number of X-ray bursts where the radius of the photosphere reached values well beyond the apparent neutron-star radius. We consider these as the secure events where the PRE occurred. Based on this histogram, we tagged an X-ray burst as a PRE event if $A_{\rm peak}/A_{\rm cool} > 1.65$. This value corresponds to the end of the tail of the main peak in the histogram.

We excluded from the final selected sample one X-ray burst (burst 92) observed from the direction of 4U 1636−536. Even though this burst satisfied the selection criteria, the measured peak flux, 1.75×10^{-8} erg s^{-1} cm^{-2}, is much lower than the fluxes reached in the rest of the burst sample and only half

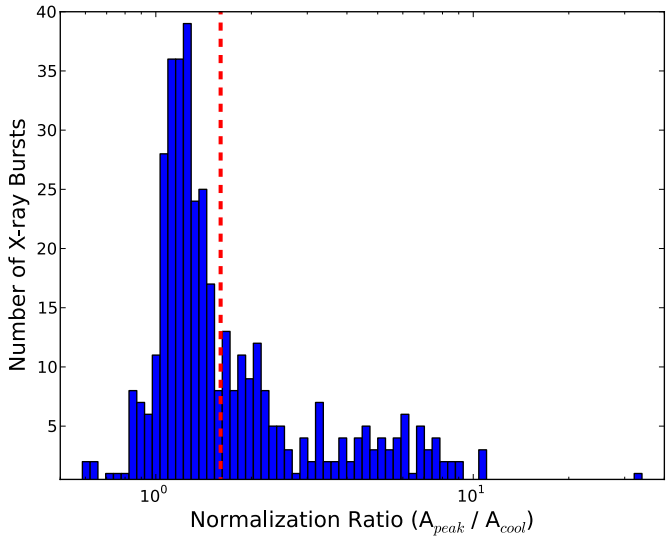

Figure 2. Ratio of the peak blackbody normalization values ($A_{\rm peak}$) found from all the X-ray bursts analyzed here to those obtained from the cooling tails ($A_{\rm cool}$) of all the X-ray bursts (Paper I). Larger ratios correspond to more distinguishable photospheric radius expansion episodes. The dashed line shows our limit between the secure and non-secure PRE events.

(A color version of this figure is available in the online journal.)

of the peak flux reached in burst ID 16, which is thought to be a hydrogen-rich burst (Galloway et al. 2006). In Table 1, we present the number of PRE bursts for each source that are obtained as a result of the full set of criteria listed above. The additional criterion, which eliminated bursts such as the one shown in the right panel of Figure 1, naturally led to numbers of secure PRE events per source that are somewhat lower than those selected by Galloway et al. (2008a). In addition, some of the difference in the number of PRE events is caused by the γ limit we imposed in the burst selection in order to minimize uncertainties related to the subtraction of the persistent flux, which we take as background. Table 1 shows the number of bursts for each source that remain after the application of these criteria.

The number of PRE events was most significantly affected by the more strict selection criteria for 4U 1728−34: 16 out of the 69 events that were tagged potentially as PRE by Galloway et al. (2008a) passed the additional criteria. This was either because the increase in the normalization was not statistically significant when compared with the apparent radius of the neutron star in the cooling tails of bursts or because the normalization showed a second increase during the cooling tail of the burst that sometimes exceeded the peak normalization during the PRE phase, as in the example shown in the right panel of Figure 1. X-ray bursts showing similar spectral evolution were previously reported by van Straaten et al. (2001) and also by Galloway et al. (2003). Given the fact that both at the peak and during the cooling tails of these bursts the normalization values are comparable to the apparent radius of the neutron star, it is possible that the variation in the blackbody normalization is caused by a significant variation in the color temperature and is not due to a PRE. This is also further supported by the fact that during the peak of these particular X-ray bursts, color temperatures were significantly higher than 2.5 keV and similar trends in the blackbody normalization were also noted in Paper I at these high temperatures. X-ray bursts showing similar spectral evolution were also seen from 4U 1702−429 and Aql X-1.

We finally explored whether PRE bursts occur only during certain spectral states of the neutron-star binaries. To this end, we used the data from Galloway et al. (2008a) to produce color–color diagrams for the burst sources and marked on these diagrams the locations of the PRE and non-PRE bursts. Figure 3 shows the soft and hard color for 4U 1728−34 and 4U 1636−536 prior to the detection of each X-ray burst. The large (red) data points correspond to PRE bursts, while the small (black) points show all other thermonuclear bursts from that source. The PRE bursts appear to occur predominantly when the sources lie near the soft vertices of their color–color diagrams (see also Muno et al. 2000). However, the regions with PRE bursts still extend across $\simeq 1/2$ of the lengths of the color–color tracks. This minimizes the possibility that the reproducibility of the inferred touchdown fluxes simply reflects the fact we are considering only very similar X-ray bursts in a very narrow range of accretion rates.

Our limit on the pre-burst flux, i.e., the requirement that $\gamma < 0.1$, excludes the brightest regions of the color–color diagram of each source and may also introduce a bias in our selection of only particular PRE bursts. This is not the case here, however, as only a very small fraction of the color–color diagram of each source corresponds to $\gamma > 0.1$ (compare, for example, the color–color diagram in Figure 3 with the entire color–color diagram of 4U 1728−34 in Figure 1 of Muno et al. 2002).

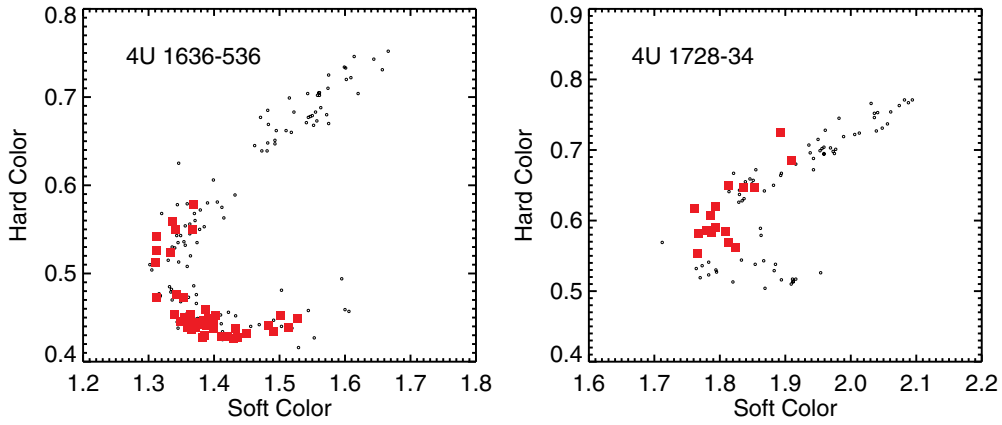

Figure 3. Positions of 4U 1636−536 (left panel) and 4U 1728−34 (right panel) on their color–color diagrams prior to the detection of an X-ray burst, using the data from Galloway et al. (2008a). Red filled squares correspond to events that show clear evidence of photospheric radius expansion. Secure PRE events appear to occur predominantly near the soft vertex of the color–color diagrams.

(A color version of this figure is available in the online journal.)

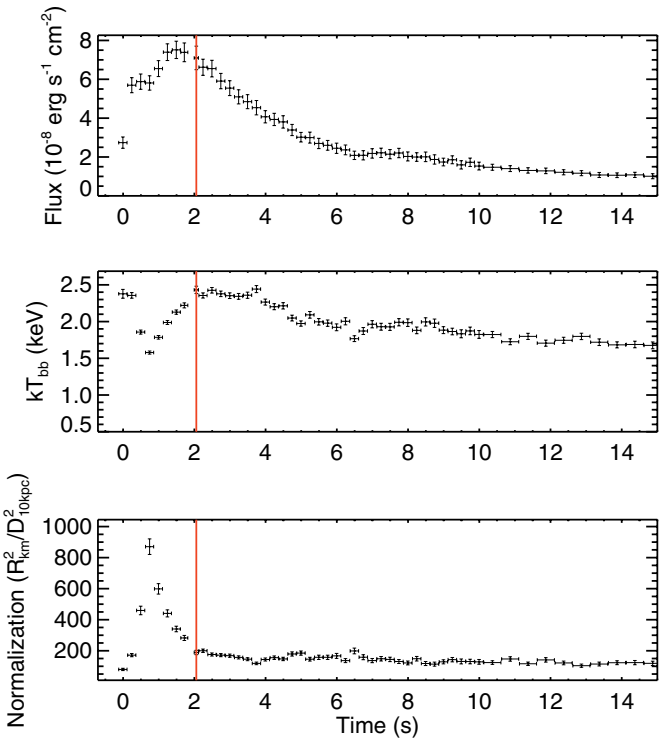

Figure 4. Example X-ray burst observed from 4U 1636−536 (burst ID 150) where the touchdown moment is not defined at the moment when the temperature reached its global maximum and the normalization its minimum but defined as the first moment when the temperature is within 1σ of the highest value.

(A color version of this figure is available in the online journal.)

4. DETERMINATION OF THE TOUCHDOWN MOMENT AND THE EDDINGTON LIMIT

We now discuss the determination of the touchdown moment and the measurement of the touchdown flux for the PRE bursts in our sample. We present here the details of the analysis for 4U 1636−536 and 4U 1728−34, which are the sources with the highest number of PRE events.

The touchdown moment is defined as the moment when the photosphere falls back onto the neutron star, which is thought to occur when the observed blackbody normalization reaches its lowest and the temperature its highest value. In a very small number of X-ray bursts, however, a statistically insignificant temperature maximum can occur several seconds past the peak flux, as in the example of the PRE burst from 4U 1636−536 shown in Figure 4. In these cases, we selected the first temperature maximum (and normalization minimum) past the peak flux, ensuring that the temperature at this point is within 1σ of its global maximum. The touchdown moments in a total of 6 out of 83 bursts from all of the sources were selected in this way.

The precise determination of the touchdown moment can also be affected by data gaps that are present in the science event mode data in some burst observations. In these cases, where a gap may have an effect on the determination of the touchdown moment, we checked whether a "burst catcher" mode with spectral information (e.g., mode CB_8ms_64M_0_249_H) was used. We found that only in six cases were there no burst catcher mode data with spectral information. For the rest of the X-ray bursts, we made use of the data in the burst catcher mode to determine the exact touchdown moments.

We fit the spectrum that we extracted at the touchdown moment for each PRE event as described in Section 2. The resulting X^2/degrees of freedom (dof) histograms for 4U 1636−536 and 4U 1728−34 are shown in Figure 5 (see Paper I for the definition of this statistic). Using the X^2/dof limits determined in Paper I, we can determine whether a particular fit is statistically acceptable or it should be excluded from further analysis. The X-ray spectra at the touchdown moments were well described with blackbody functions, leading in general to small X^2/dof values. Therefore, applying the X^2/dof limits forced us to exclude only one X-ray burst from 4U 1705−44 (burst 1) and two X-ray bursts from 4U 1636−536 (bursts 3 and 9).

5. SYSTEMATIC UNCERTAINTIES IN THE EDDINGTON LIMIT

In this section, we will address the formal and systematic uncertainties in the touchdown fluxes obtained from the PRE bursts of each source. As before, we will first focus on the two sources with the highest number of bursts to present the details of the method and then extend our analysis to the rest of the sample. We will start by discussing our determination of the bolometric flux at touchdown and its formal uncertainty. We will then explore whether the different PRE bursts from the same source reach a touchdown flux that remains statistically constant between bursts.

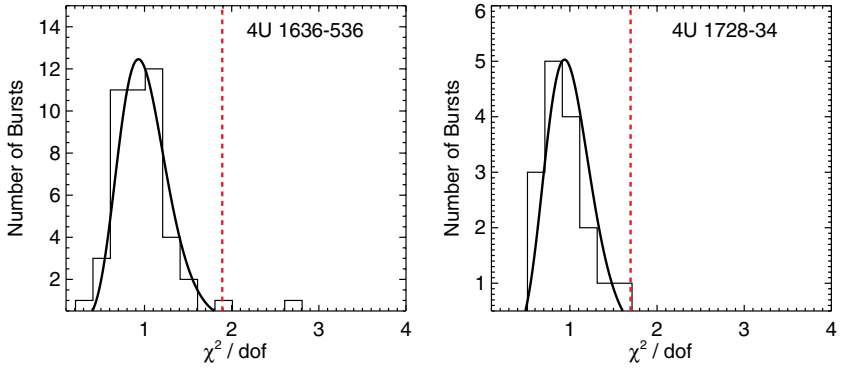

Figure 5. Distributions of X^2/dof values obtained from model fits to the X-ray spectra extracted at the touchdown moments of X-ray bursts observed from 4U 1636−536 (left panel) and 4U 1728−34 (right panel). The solid lines show the expected distributions for the number of degrees of freedom in the fits, and the dashed lines show the highest values of X^2/dof that were considered as statistically acceptable in Paper I using the spectral fits of the cooling tails of all the X-ray bursts for each source. During touchdown the spectra are described well by blackbody functions.

(A color version of this figure is available in the online journal.)

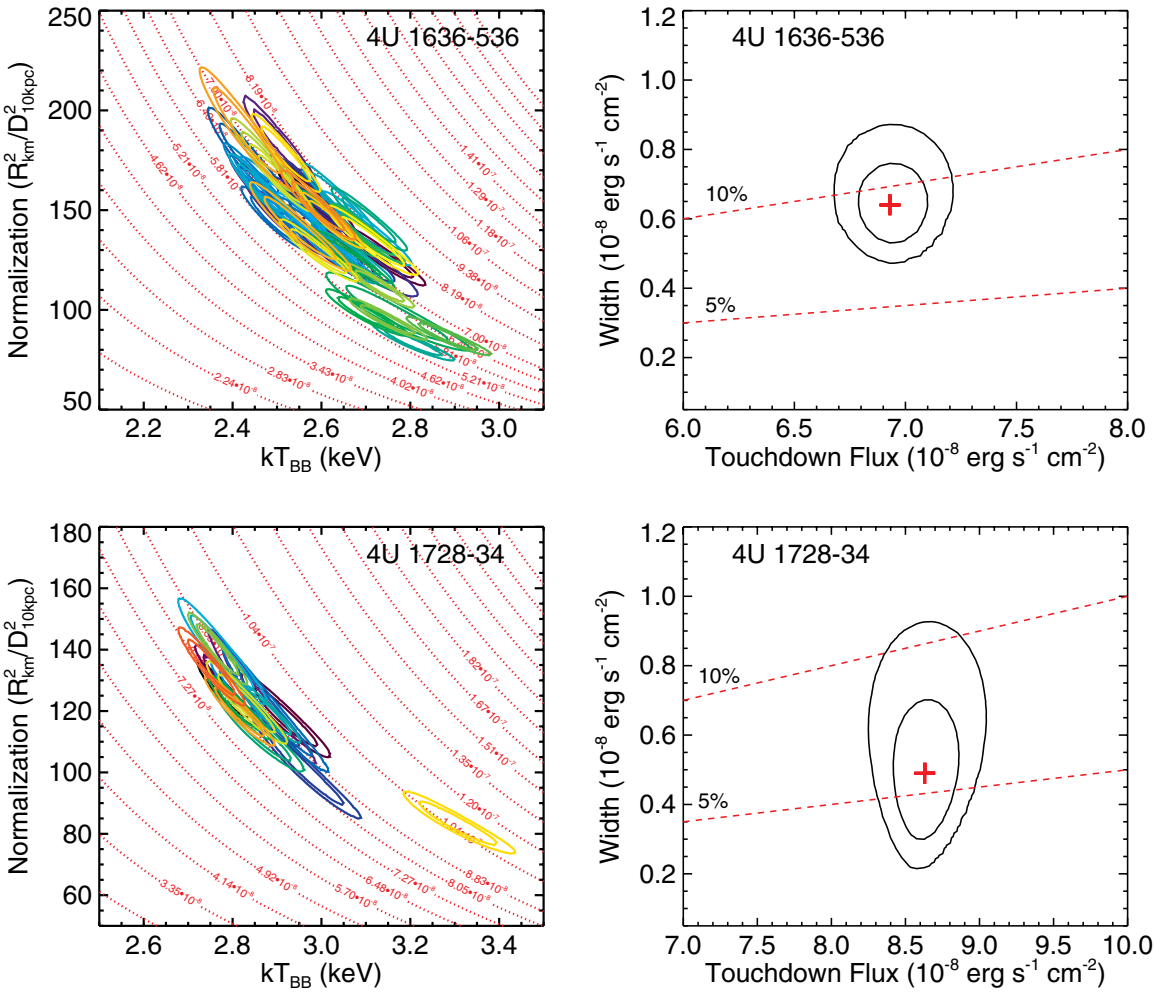

Figure 6. Left panels: 68% and 95% confidence contours of the blackbody normalization and temperature obtained from fitting the X-ray spectra at the touchdown moments of each PRE burst observed from 4U 1636−536 and 4U 1728−34. The dotted red lines show contours of constant bolometric flux. Right panels: 68% and 95% confidence contour of the parameter of an assumed underlying Gaussian distribution of touchdown fluxes. The width of the underlying distribution reflects the systematic uncertainty in the measurements. The dashed red lines show the width when the systematic uncertainty is 5% and 10% of the mean touchdown flux.

(A color version of this figure is available in the online journal.)

For each burst, the bolometric flux at touchdown is obtained from the combination of the blackbody temperature and normalization. Figure 6 shows the 68% and 95% confidence contours of the blackbody normalization and temperature inferred from fitting the X-ray spectra obtained during the touchdown moment for 4U 1728−34 and 4U 1636−536. We also plot in these figures contours of constant bolometric flux, shown as dotted (red) lines. Even though the uncertainties in the normalization and temperature are correlated, the bolometric flux in each burst is well constrained. Furthermore, as Figure 6 shows, the individual confidence contours from each burst appear to be in very good statistical agreement with each other for both sources.

The distribution of inferred bolometric fluxes at touchdown is expected to have a finite width both because of measurement uncertainties and because of the possible variations in the physical conditions that determine the emerging flux during a PRE burst. The measurement uncertainties include formal uncertainties from counting statistics, the uncertainties in the bolometric correction, the subtraction of the background emission, and the determination of the touchdown moment. Anisotropies in the bursts, variations in the composition and the reflection off the accretion flow (e.g., Galloway et al. 2004, 2006), and variations in the Compton upscattering in the converging inflow prior to touchdown are some of the physical mechanisms that can contribute to the intrinsic spread.

For the high temperatures observed during the touchdown phases of the bursts, most of the burst spectrum falls within the *RXTE* energy range, resulting in bolometric corrections that are at most 7% (Galloway et al. 2008a). Therefore, any uncertainties in the bolometric correction can only introduce minimal spread to the width of the observed touchdown fluxes. Uncertainties in the determination of the touchdown moment are also expected to be of the same magnitude since the fluxes in the nearby time bins differ typically by less than 10% (see, e.g., Figures 2 and 4). Our 10% limit on the pre-burst persistent flux bounds the uncertainties introduced by our subtraction of the background. We can also estimate the expected variations due to the Compton upscattering in the converging flow: this effect scales as v/c and can, therefore, introduce an uncertainty at most of the order of 10% (van Paradijs & Stollman 1984). On the other hand, variations in the isotropy or the composition of the bursts can, in principle, generate larger spread in the touchdown fluxes.

Our goal is to quantify the widths of the underlying distributions of touchdown fluxes, which we will call systematic

Table 2
Measured Touchdown Flux Values from PRE Events

Source Name	BID[a]	MJD[a]	Touchdown Flux[b]	Normalization Ratio
4U 0513−40	6	53442.08752	1.32 ± 0.07	3.30
	7	54043.68856	1.06 ± 0.06	9.00
4U 1636−53	1	50445.94404	7.25 ± 0.15	6.63
	4	50448.73395	7.09 ± 0.15	6.19
	6	51044.48934	7.43 ± 0.19	4.95
	7	51045.15288	7.64 ± 0.23	9.82
	10	51297.07198	7.55 ± 0.21	8.21
	12	51339.24688	7.23 ± 0.18	4.82
	13	51347.98824	6.35 ± 0.16	4.16
	14	51348.72984	6.86 ± 0.15	5.01
	15	51350.79575	6.52 ± 0.14	5.12
	20	51710.21233	7.81 ± 0.20	7.24
	21	51765.05463	6.28 ± 0.20	5.71
	22	51765.37284	7.00 ± 0.40	5.60
	23	51768.98081	7.52 ± 0.18	5.90
	24	51820.98112	7.24 ± 0.17	5.47
	25	51853.18194	6.64 ± 0.22	3.07
	26	51860.75171	6.02 ± 0.16	3.74
	27	51937.11612	6.70 ± 0.16	5.65
	28	51941.87558	6.43 ± 0.16	3.74
	29	51942.10024	6.62 ± 0.23	5.26
	30	52004.71326	6.65 ± 0.17	7.54
	31	52029.22818	6.74 ± 0.16	4.04
	34	52075.13477	7.97 ± 0.25	9.89
	38	52149.27871	6.35 ± 0.15	2.67
	45	52182.61618	8.11 ± 0.22	5.10
	49	52283.01850	6.93 ± 0.18	4.36
	50	52273.69081	5.56 ± 0.17	7.02
	61	52286.05404	8.36 ± 0.20	5.01
	62	52286.55466	7.42 ± 0.20	6.78
	68	52287.52190	6.15 ± 0.33	8.32
	72	52288.51431	6.85 ± 0.20	6.28
	79	52288.97438	5.60 ± 0.17	6.52
	86	52289.29282	7.89 ± 0.21	5.92
	87	52289.97694	6.43 ± 0.20	8.64
	88	52304.96314	5.84 ± 0.16	4.59
	94	52310.93185	6.69 ± 0.17	7.21
	110	52316.73272	7.06 ± 0.20	4.24
	111	53516.31312	7.05 ± 0.17	4.47
	122	52551.25121	6.26 ± 0.17	1.89
	136	53516.31312	7.81 ± 0.24	10.17
	137	53524.38883	7.70 ± 0.20	7.47
	148	53592.23376	7.33 ± 0.17	5.69
	149	53596.08782	6.37 ± 0.22	4.62
	150	53598.07334	7.12 ± 0.26	6.37
	168	53688.95192	7.36 ± 0.20	7.32
4U 1702−429	19	52957.62907	9.05 ± 0.26	3.12
4U 1705−44	5	50542.50287	4.13 ± 0.13	2.63
4U 1724−307	2	53058.40140	4.56 ± 0.13	1.76
	3	53147.21828	6.01 ± 0.17	1.67
4U 1728−34	2	50128.88220	8.13 ± 0.17	2.30
	21	50718.47163	9.21 ± 0.27	3.04
	22	50718.66257	8.41 ± 0.16	4.47
	38	51133.42394	8.88 ± 0.23	3.32
	39	51133.67299	8.36 ± 0.21	2.46
	41	51134.57233	8.97 ± 0.23	2.35
	48	51204.00117	8.50 ± 0.19	2.65
	49	51204.12990	8.86 ± 0.28	1.80
	51	51206.14068	8.86 ± 0.19	4.05
	53	51209.91806	8.16 ± 0.26	1.86
	54	51210.08245	8.18 ± 0.18	1.85
	55	51213.93849	8.80 ± 0.19	2.04
	69	51443.01361	8.43 ± 0.24	1.66
	83	51949.12600	10.68 ± 0.38	1.99
	85	52007.61313	8.09 ± 0.20	2.03
	86	52008.08709	8.29 ± 0.20	3.38
KS 1731−260	8	51235.71747	4.65 ± 0.13	4.49
	9	51236.72580	4.75 ± 0.13	3.90
4U 1735−44	6	50963.42981	3.27 ± 0.12	2.68
	7	50963.48944	3.07 ± 0.10	2.26
SAX J1748.9−2021	1	52190.38947	4.52 ± 0.14	33.99
	2	52190.46882	3.54 ± 0.12	3.37
SAX J1750.8−2900	2	52011.59758	5.63 ± 0.16	1.86
	3	52014.71002	5.58 ± 0.19	2.13
Aql X-1	4	50508.97681	11.95 ± 0.19	3.91
	5	50696.52359	12.16 ± 0.19	5.56
	10	51332.77990	11.55 ± 0.24	7.52
	19	51856.15690	8.45 ± 0.25	7.36
	28	52324.99055	12.09 ± 0.21	6.22
	29	52347.18234	6.38 ± 0.18	2.24

Notes.
[a] Burst IDs and burst start times are adopted from Galloway et al. (2008a).
[b] Values are given in units of 10^{-8} erg cm^{-2} s^{-1} and are calculated using Equation (3) of Galloway et al. (2008a).

uncertainties that are potentially caused by any of these effects. In order to achieve this, we need an approach that is valid both in the limit when the formal uncertainty for each measurement is much smaller than the variance of the distribution of their central values and in the opposite extreme. In the first case, the variance of the mean values is practically equal to the width of the underlying distribution. In the opposite limit, when the formal uncertainties in each measurement are comparable to or larger than the variance of the mean values, one could compute the systematic uncertainty $\sigma_{\rm sys}$ by subtracting in quadrature the formal uncertainty $\sigma_{\rm form}$ from the variance $\sigma_{\rm var}$, i.e.,

$$\sigma_{\rm sys}^2 = \sigma_{\rm var}^2 - \sigma_{\rm form}^2. \quad (1)$$

This can be carried out only if the formal uncertainties in each measurement are the same.

In our sample, however, each flux measurement has a different formal uncertainty and the uncertainty in each measurement is sometimes comparable to and sometimes smaller than the variance of the mean flux values for different sources. In order to properly account for this, we follow here the Bayesian analysis method discussed in Paper I that allows us to determine the intrinsic spread of touchdown fluxes.

In the Bayesian analysis, we first determine the formal uncertainties of the measured bolometric fluxes for each burst and each source using the confidence contours shown in Figure 6 and report these in Table 2. We model the underlying distribution of touchdown fluxes as a Gaussian. The observed distribution is a convolution of the underlying distribution with the individual formal uncertainties for each burst that we measured above. We then use the Bayesian technique presented in Paper I to determine the most probable value F_0 and width σ of the underlying distribution of touchdown fluxes for each source. Figure 7 shows the histogram of observed touchdown fluxes and the most probable underlying distribution for the two sources 4U 1636−536 and 4U 1728−34. The right panels of Figure 6 show the full confidence contours for the parameters of these

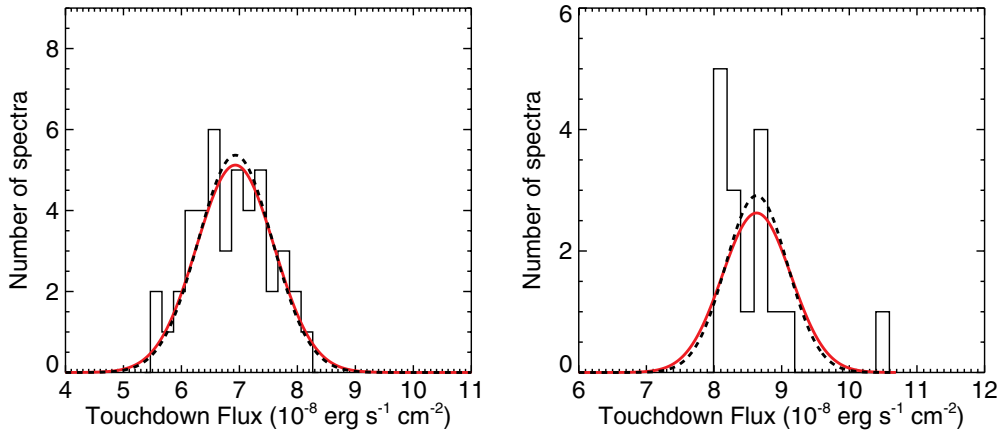

Figure 7. Histogram of measured touchdown fluxes for 4U 1636−536 (left panel) and 4U 1728−34 (right panel). The red solid line shows the underlying Gaussian distribution as inferred from the Bayesian analysis. The black dashed curve shows the distribution of the touchdown fluxes when the observational uncertainties are taken into account. The width of the underlying distribution reflects the systematic uncertainty in the measurements.

(A color version of this figure is available in the online journal.)

Table 3
The Measured Touchdown Fluxes

Source Name	Touchdown Flux[a]	σ_{sys}[b]	σ_{form}[c]
4U 0513−401	1.19	0.11	0.06
4U 1636−536	6.93	0.64	0.20
4U 1724−307	5.29	0.70	0.16
4U 1728−34	8.63	0.46	0.22
KS 1731−260	4.71	n/a	0.13
4U 1735−44	3.15	n/a	0.11
SAX J1748.9−2021	4.03	0.54	0.13
SAX J1750.8−2900	5.61	0.01	0.17
Aql X-1	10.44	2.22	0.21

Notes.
[a] Fluxes and uncertainties are in units of 10^{-8} erg s^{-1}cm^{-2}.
[b] These reflect the most probable widths of the underlying distributions.
[c] These reflect the uncertainties in measuring the most probable values of the underlying distributions.

Table 4
Fractional Differences of Pairs of Touchdown Fluxes

Source Name	R[a]
4U 0513−401	0.218 ± 0.077
4U 1724−307	0.274 ± 0.039
KS 1731−260	0.021 ± 0.039
4U 1735−44	0.063 ± 0.049
SAX J1748.9−2021	0.243 ± 0.045
SAX J1750.8−2900	0.009 ± 0.044

Note. [a] Defined as $R \equiv 2|F_2 - F_1|/(F1 + F2)$.

underlying distributions. Even though the most probable values for the touchdown fluxes can be determined within a few percent, there is clear evidence for a 5%–10% spread, which we attribute to the physical mechanisms discussed above.

In Figures 8 and 9 and Table 3, we show the results of the same analysis for all the other sources. Naturally, the intrinsic widths in the touchdown fluxes for the sources with very few bursts are more difficult to determine. In all cases except Aql X-1, however, the level of systematic uncertainties is not inconsistent with the 5%–10% level inferred for the two sources with many bursts. Notably, Aql X-1 is also the source with the largest variation in the apparent surface area during the cooling tails of its bursts (Paper I).

Even though it is difficult to determine the shape and width of the underlying distribution for any of the sources with only two PRE bursts, it is worth noting that for three out of the six cases, the fractional difference between the two touchdown fluxes, F_1 and F_2, as defined by

$$R \equiv \frac{2(F_1 - F_2)}{F_1 + F_2}\,, \qquad (2)$$

is less than 7%. It would be very unlikely for the underlying distribution of touchdown fluxes in each source to be much broader than this level and for half of the randomly picked pairs of touchdown fluxes to be within 7%.

In the following section, we quantify this statement by making the assumption that all sources have a distribution of touchdown fluxes with the same fractional width. We use the R value for each of the burst pairs given in Table 4 to show that the most likely fractional width of the underlying distribution of touchdown fluxes is 11^{+5}_{-3}% (68% confidence level).

6. SYSTEMATIC UNCERTAINTIES IN SOURCES WITH FEW PRE BURSTS

Our aim here is to estimate the most likely fractional dispersion of touchdown fluxes in X-ray bursters that can reproduce the observed R values for the six sources in our sample for which we have only two observations of PRE bursts each. Because of the small number of data points available, we will assume that the underlying distribution of touchdown fluxes in each source is a Gaussian, with the same fractional dispersion σ, i.e.,

$$P_{td}(F/F_0;\sigma) = \frac{1}{\sqrt{2\pi\sigma^2}} \exp\left[-\frac{(F/F_0 - 1)^2}{2\sigma^2}\right], \qquad (3)$$

where F is the touchdown flux of each burst and F_0 is the mean touchdown flux for each source.

If we draw a random pair of touchdown fluxes F_1 and F_2 from this distribution and calculate their fractional difference R (Equation (2)), then the distribution of the R values will be

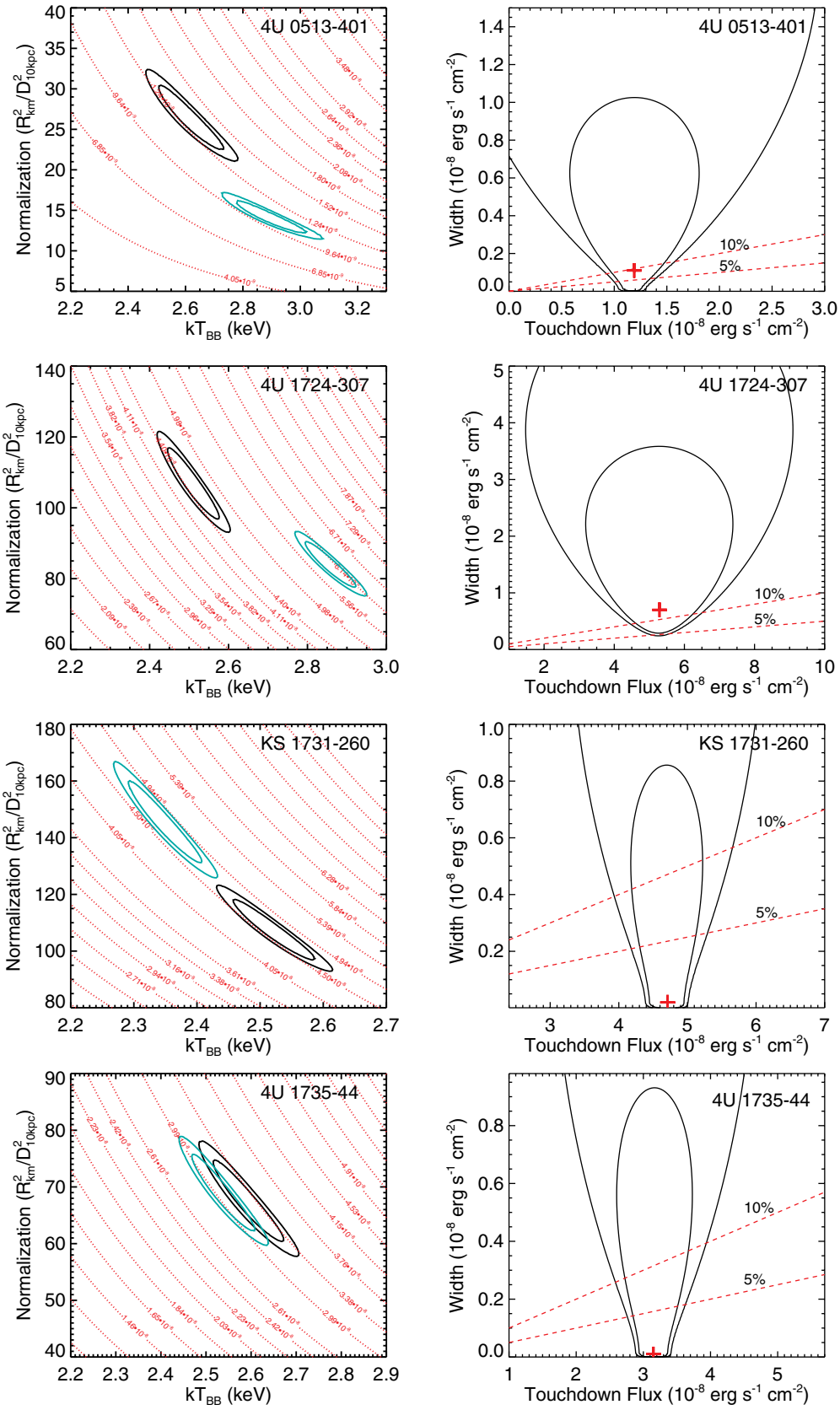

Figure 8. Same as Figure 6 but for the sources 4U 0513−401, 4U 1724−307, KS 1731−26, and 4U 1735−44.
(A color version of this figure is available in the online journal.)

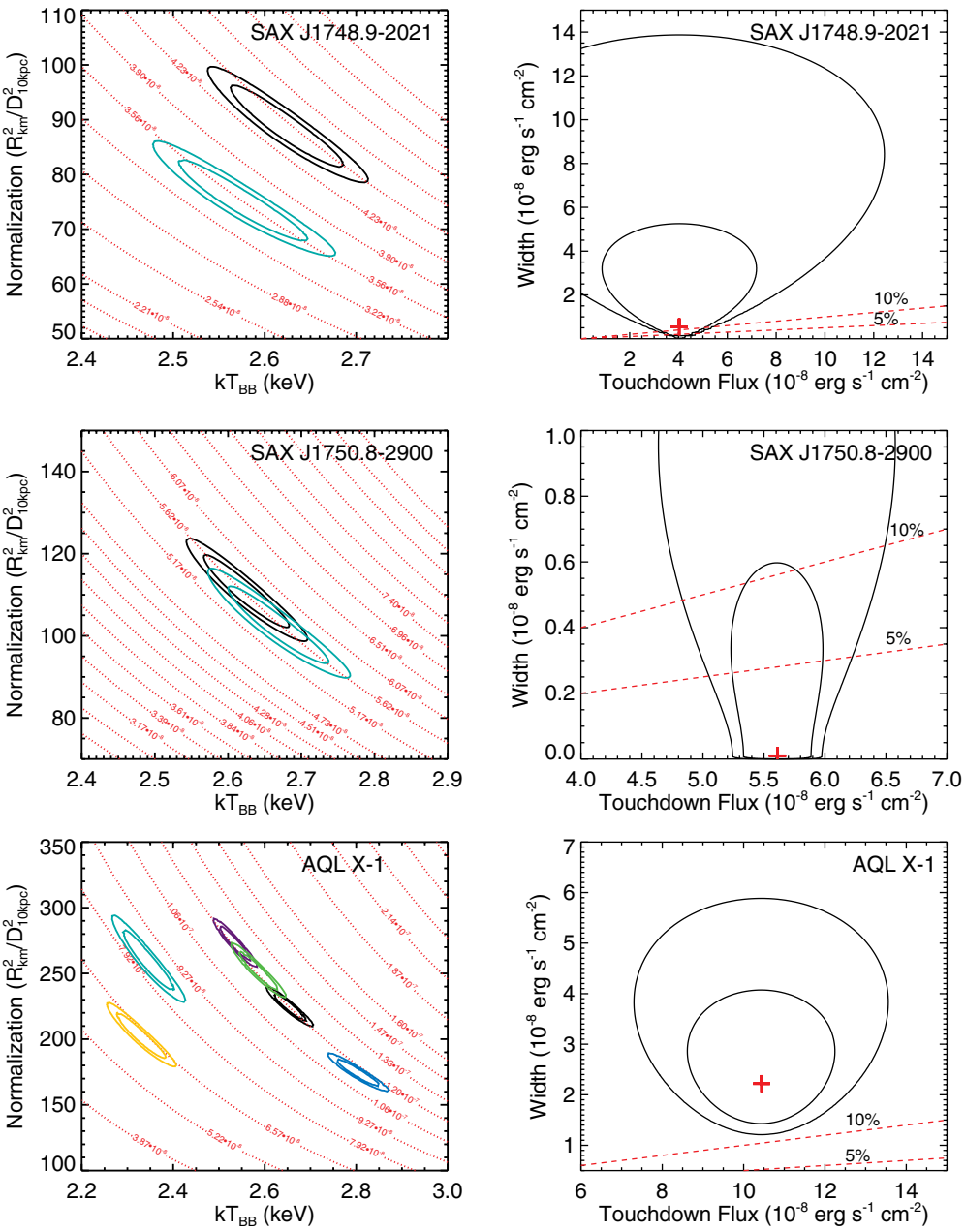

Figure 9. Same as Figure 8 but for the sources SAX J1750.8−2900, SAX J1748.9−2021, and Aql X-1.
(A color version of this figure is available in the online journal.)

given by

$$P(R;\sigma) = C \int P_{\rm td}\left(\frac{F}{F_0};\sigma\right)\left\{P_{\rm td}\left[\left(\frac{2-R}{2+R}\right)\frac{F}{F_0};\sigma\right] + P_{\rm td}\left[\left(\frac{2+R}{2-R}\right)\frac{F}{F_0};\sigma\right]\right\} d\left(\frac{F}{F_0}\right), \quad (4)$$

where C is an appropriate normalization constant. The distribution $P(R;\sigma)$ peaks at $R = 0$ for all values of σ and drops quickly to zero such that the median value of R for this distribution is $R_{50\%} = \sigma$. Given that half of our six sources with only pairs of PRE bursts have R values that are less than 7%, we expect that the most probable value of the fractional dispersion of their touchdown fluxes will be of the same order.

For each source with a pair of PRE bursts, we assign a Gaussian likelihood of R values, taking into consideration the fact that the R value is always positive, as

$$P_{\rm obs}\left(R;\, R_0^i, \sigma_R^i\right) = \frac{1}{\sqrt{2\pi}\sigma_R^i}\left\{\exp\left[-\frac{\left(R-R_0^i\right)^2}{2\left(\sigma_R^i\right)^2}\right] + \exp\left[-\frac{\left(-R-R_0^i\right)^2}{2\left(\sigma_R^i\right)^2}\right]\right\}, \quad R > 0, \quad (5)$$

with a most likely value R_0^i and a dispersion σ_R^i given in Table 4. The likelihood $P_{\rm obs}(R, R_0^i, \sigma_R^i)$ for each source with a pair of PRE bursts is shown in Figure 10.

The likelihood of observing the $N = 6$ pairs of R values with the likelihood shown in Figure 10, given an underlying

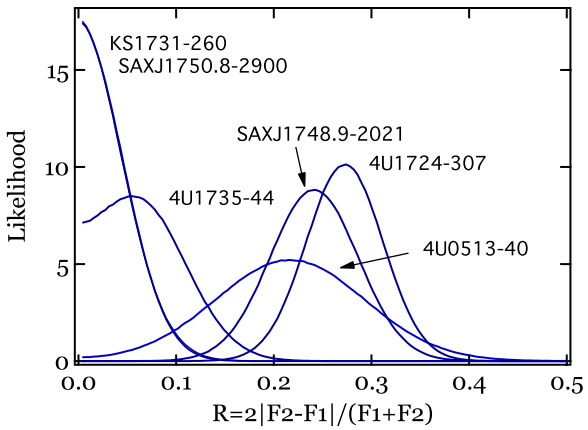

Figure 10. Likelihood of the fractional difference R between the touchdown fluxes, F_1 and F_2, of pairs of bursts in sources with only two PRE bursts.
(A color version of this figure is available in the online journal.)

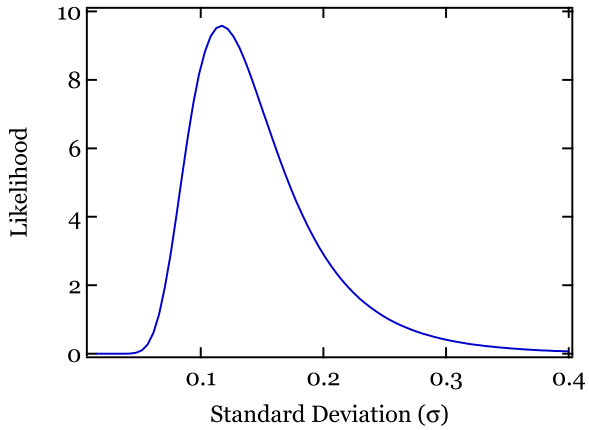

Figure 11. Posterior probability over the fractional width σ of the touchdown flux distribution for the six sources that exhibit only a pair of PRE bursts each.
(A color version of this figure is available in the online journal.)

fractional dispersion σ, is

$$P(\text{data}|\sigma) = \prod_{i=1}^{N} \int P(R;\sigma) P_{\rm obs}\left(R;\, R_0^i,\, \sigma_R^i\right) dR\ . \qquad (6)$$

Using Bayes' theorem, we can then calculate the likelihood of each fractional dispersion σ given the data as

$$P(\sigma|\text{data}) = C' P(\text{data}|\sigma) P_\sigma(\sigma)\ , \qquad (7)$$

where C' is another appropriate normalization constant and we take the prior probability over all possible fractional dispersions $P_\sigma(\sigma)$ to be constant over the range of interest.

Figure 11 shows the posterior probability over the fractional dispersion σ that is consistent with the six observed R values. The most likely fractional dispersion of touchdown fluxes for our sample of six sources with only one pair of observed PRE bursts each is $11^{+5}_{-3}\%$, where we determined the quoted uncertainty at the 68% level in the asymmetric probability distribution.

7. DISCUSSION

We used the *RXTE* archive of thermonuclear X-ray bursts to select the bursts that show clear evidence for PRE. We determined systematically the touchdown moment of each burst and inferred the bolometric flux at that point in the burst. We then used a Bayesian technique to infer the most probable value and the width of the distribution of touchdown fluxes in each source. In the two sources with more than a few bursts, the inferred width is within 5%−10% of the most probable touchdown flux. In the six sources with only one pair of PRE bursts each, the width of the underlying distribution is consistent with being at a similar level. When the latter group of sources is taken as a representative sample, the most likely fractional width of their touchdown fluxes is $\simeq$11%. The only clear exception is Aql X-1, where the systematic uncertainties exceed $\sim$20%.

As we explored in Section 5, the distribution of the touchdown fluxes is expected to have a finite width for a number of observational and physical reasons. For a number of these effects, we were able to estimate that they introduce a 5%−10% level of systematic uncertainty in the fluxes. The two unknowns that potentially introduce larger systematic uncertainties are the asymmetry of the PRE event and the composition of the material at the photosphere. Our results show, however, that even these unknowns do not introduce uncertainties larger than 10%.

The PRE bursts allow us to measure the Eddington limit at the surface of the neutron star for each source. Determining the Eddington limit requires an absolute flux measurement, which is affected by the overall flux calibration of the X-ray detector used. Such calibrations are notoriously difficult to achieve and are usually based on a particular set of assumptions regarding the spectrum and variability of the Crab Nebula (Jahoda et al. 2006; see also Toor & Seward 1974; Kirsch et al. 2005; Weisskopf et al. 2010). Any bias in the absolute flux calibration cannot increase the spread of touchdown fluxes that we infer here for each source. However, it can affect the mean touchdown flux, which, in turn, enters into the measurement of neutron-star masses and radii. We will quantify the potential systematic uncertainties introduced by the absolute flux calibration of PCA in Paper III of this series.

It is also important to emphasize here that our results are based on a statistical analysis of the entire sample of PRE bursts per source and do not preclude the possibility that any one individual burst may show a rather different touchdown flux. Indeed, there is at least one burst observed from 4U 1636−536 (ID 16),[4] for which the touchdown flux was smaller than the average value by a factor of 1.7 (Galloway et al. 2006). In this particular case, a variation in the hydrogen mass fraction from $X = 0$ to $X = 0.7$ between the bursts has been considered as a natural explanation of the difference in touchdown fluxes (Sugimoto et al. 1984; Galloway et al. 2006). The fact that such outliers may and do exist makes it essential that proper statistical tools are used in all inferences based on measurements of the touchdown fluxes of PRE bursts.

In conclusion, our results indicate that the systematic uncertainties in the measurements of touchdown fluxes in radius expansion bursts from low-mass X-ray binaries are within $\simeq$10%, for nearly the entire source sample. Such systematic uncertainties do not preclude, in and of themselves, neutron-star mass–radius measurements with high enough precision to distinguish between different equations of state of neutron-star matter.

We thank the anonymous referee for constructive suggestions. This work was supported by NASA ADAP grant NNX10AE89G

[4] Although this burst is a PRE event and we find a touchdown flux that is very similar to the one in Galloway et al. (2006), it is not included in this study because the persistent flux of the binary before this X-ray burst was higher than our limit.

and Chandra Theory grant TMO-11003X. D.P. was supported by the NSF CAREER award NSF 0746549 and Chandra Theory grant TMO-11003X. This research has made use of data obtained from the High Energy Astrophysics Science Archive Research Center (HEASARC), provided by NASA's Goddard Space Flight Center.

REFERENCES

Arnaud, K. A. 1996, in ASP Conf. Ser. 101, Astronomical Data Analysis Software and Systems V, ed. G. H. Jacoby & J. Barnes (San Francisco, CA: ASP), 17
Basinska, E. M., Lewin, W. H. G., Sztajno, M., Cominsky, L. R., & Marshall, F. J. 1984, ApJ, 281, 337
Damen, E., Magnier, E., Lewin, W. H. G., et al. 1990, A&A, 237, 103
Ebisuzaki, T. 1987, PASJ, 39, 287
Ebisuzaki, T., Hanawa, T., & Sugimoto, D. 1983, PASJ, 35, 17
Galloway, D. K., Cumming, A., Kuulkers, E., et al. 2004, ApJ, 601, 466
Galloway, D. K., Muno, M. P., Hartman, J. M., Psaltis, D., & Chakrabarty, D. 2008a, ApJS, 179, 36
Galloway, D. K., Özel, F., & Psaltis, D. 2008b, MNRAS, 387, 268
Galloway, D. K., Psaltis, D., Chakrabarty, D., & Muno, M. P. 2003, ApJ, 590, 999
Galloway, D. K., Psaltis, D., Muno, M. P., & Chakrabarty, D. 2006, ApJ, 639, 1033
Güver, T., Özel, F., Cabrera-Lavers, A., & Wroblewski, P. 2010a, ApJ, 712, 964
Güver, T., Psaltis, D., & Özel, F. 2012, ApJ, 747, 76 (Paper I)
Güver, T., Wroblewski, P., Camarota, L., & Özel, F. 2010b, ApJ, 719, 1807
Houck, J. C., & Denicola, L. A. 2000, in ASP Conf. Ser. 216, Astronomical Data Analysis Software and Systems IX, ed. N. Manset, C. Veillet, & D. Crabtree (San Francisco, CA: ASP), 591
in't Zand, J. J. M., & Weinberg, N. N. 2010, A&A, 520, A81
Jahoda, K., Markwardt, C. B., Radeva, Y., et al. 2006, ApJS, 163, 401
Kato, M. 1983, PASJ, 35, 33
Keek, L., Galloway, D. K., in't Zand, J. J. M., & Heger, A. 2010, ApJ, 718, 292
Kirsch, M. G., Briel, U. G., Burrows, D., et al. 2005, Proc. SPIE, 5898, 22
Kuulkers, E., den Hartog, P. R., in't Zand, J. J. M., et al. 2003, A&A, 399, 663
Lewin, W. H. G., van Paradijs, J., & Taam, R. E. 1993, Space Sci. Rev., 62, 223
Muno, M. P., Fox, D. W., Morgan, E. H., & Bildsten, L. 2000, ApJ, 542, 1016
Muno, M. P., Remillard, R. A., & Chakrabarty, D. 2002, ApJ, 568, L35
Özel, F., Güver, T., & Psaltis, D. 2009, ApJ, 693, 1775
Paczynski, B., & Proszynski, M. 1986, ApJ, 302, 519
Sugimoto, D., Ebisuzaki, T., & Hanawa, T. 1984, PASJ, 36, 839
Toor, A., & Seward, F. D. 1974, AJ, 79, 995
van Paradijs, J. 1978, Nature, 274, 650
van Paradijs, J. 1979, ApJ, 234, 609
van Paradijs, J., & Stollman, G. M. 1984, A&A, 137, L12
van Straaten, S., van der Klis, M., Kuulkers, E., & Méndez, M. 2001, ApJ, 551, 907
Weisskopf, M. C., Guainazzi, M., Jahoda, K., et al. 2010, ApJ, 713, 912
Wilms, J., Allen, A., & McCray, R. 2000, ApJ, 542, 914